

Ferroelectric-HfO₂/Oxide Interfaces, Oxygen Distribution Effect and Implications for Device Performance

Notes: we have identified a mistake in the original version of manuscript entitled “Unexpected enhancement of ferroelectricity in HfO₂ on SiO₂ and GeO₂”, which will directly compromise the outcome and affect the conclusion presented in the original manuscript. To be specific, we noticed that this model had not been built with symmetric oxygen distribution at the two interfaces in the supercell structure, but with two more oxygen ions at the Hf-interface than at the O-interface. This asymmetric oxygen distribution directly translates to additional net dipole across fe-HfO₂ in the direction that opposes depolarizing field. Because this built-in field is intense, the overall field across fe-HfO₂ tends to enhance its polarization. After revising this model to the one having symmetric oxygen distribution, depolarizing field emerges in fe-HfO₂, similar to the cases in other fe-HfO₂/oxide systems. Therefore, the originally claimed unexpected enhancement of HfO₂ ferroelectricity is an artefact. As will be discussed in the revised manuscript, however, asymmetric oxygen distribution is highly relevant for fe-HfO₂-based devices.

Shihui Zhao¹⁺, Bowen Li²⁺, Yuzheng Guo³, Huanglong Li^{*2,4}

¹ School of Materials Science and Engineering, Tsinghua University, Beijing, 100084, China ² Department of Precision Instrument, Center for Brain Inspired Computing Research, Tsinghua University, Beijing, 100084, China ³ College of Engineering, Swansea University, SA1 8EN, Swansea, UK ⁴ Chinese Institute for Brain Research, Beijing, 102206, China

⁺equal contributions

*Email: li_huanglong@mail.tsinghua.edu.cn

Abstract

Atomic-scale understanding of HfO₂ ferroelectricity is important to help address many challenges in developing reliable and high-performance ferroelectric HfO₂ (fe-HfO₂) based devices. Though investigated from different angles, a factor that is real device-relevant and clearly deserves more attention has largely been overlooked by previous research, namely, the fe-HfO₂/dielectric interface. Here, we investigate the electronic structures of several typical interfaces formed between ultrathin fe-HfO₂ and oxide dielectrics in the sub-3-nm region. We find that interface formation introduces strong depolarizing fields in fe-HfO₂, which is detrimental for ferroelectric polarization but can be a merit if tamed for tunneling devices, as recently demonstrated. Asymmetric oxygen distribution-induced polarity, intertwined with ferroelectric polarization or not, is also investigated as a relevant interfacial effect in real device. Though considered detrimental from certain aspects, such as inducing build-in field (independent of ferroelectric polarization) and exacerbating depolarization (intertwined with ferroelectric polarization), it can be partly balanced out by other effects, such as annealing (extrinsic) and polarity-induced defect formation (intrinsic). This work provides insights into ferroelectric-HfO₂/dielectric interfaces and some useful implications for the development of devices.

The replacement of SiO₂ with high-K HfO₂ as the gate insulator in 2007 has been considered as one of the biggest redesign of the transistor technology¹, enabling continuous down-scaling of the transistor according to the prediction of Gordon Moore². Today, aggressive transistor scaling down to 3nm-scale is on the way³ at which the semiconductor community is becoming increasingly concerned about the ending of Moore's law. Reinvention of the device technology is imperatively called for⁴.

In 2011, a group of German researchers discovered in Si-doped HfO₂ unexpected ferroelectricity^{5, 6}, a rare materials property that has previously only been found in complex crystals, such as perovskites, which are unfortunately not CMOS-compatible. Because HfO₂ had already been a key enabler of the high-K-metal-gate technology for transistors, this discovery has led to a re-emergence of intensive research interest in ferroelectric devices, including negative-capacitance (NC) transistor⁷⁻¹⁰, ferroelectric memory transistor (or fe-transistor)¹¹⁻¹⁴ and ferroelectric tunneling junction (FTJ) nonvolatile memory^{15, 16}.

Although it is the intrinsic ferroelectricity in HfO₂ that underpins the workings of these devices, ferroelectric HfO₂ (fe-HfO₂) cannot be considered in isolation, but rather the characterized device performance reflects the entire system of the component films and the interfaces between them¹⁷. In the past, extensive investigations on ferroelectric/electrode interfaces have been conducted. Ferroelectric/electrode interfaces influence device performance in many key aspects, including critical film thickness (power and scalability relevant)¹⁸, field-cycling behavior¹⁹, tunneling electroresistance (TER, for FTJ)²⁰, and so on. In addition to ferroelectric/electrode interfaces, it is not hard to find that fe-HfO₂ is most often used in combination with another non-ferroelectric dielectric in a real device for practical reasons, giving rise to fe-HfO₂/dielectric interface. For example, NC-transistor typically uses series fe-HfO₂/dielectric gate capacitor²¹⁻²⁵ to provide sufficient capacitance matching and maintain the overall gate capacitance positive⁷⁻¹⁰, and fe-transistor typically uses fe-HfO₂/dielectric double-layer, in particular, fe-HfO₂/SiO₂²⁶⁻³⁰, for improved quality of the gate stack/semiconductor interface³¹, and in FTJ fe-HfO₂/dielectric double-layer³² can be used to achieve enhanced TER³³.

More broadly, dielectric substrates are very common for the growth of ferroelectric thin films. They interact intimately, so much so that this has usually been taken for granted. In a recent report on the counterintuitive enhancement of ferroelectricity in 1-nm ultrathin Zr-doped HfO₂ grown on SiO₂/Si³⁴, the formation of the fe-HfO₂/SiO₂ interface has only been mentioned marginally.

Furthermore, ferroelectric/dielectric interfaces are the places where electronic charge degree of freedom is strongly coupled to ionic lattice degree of freedom, creating various novel emergent phenomena, such as the formation of two-dimensional electron/hole gas (2DEG/2DHG)³⁵⁻³⁷. In this respect, ferroelectric/dielectric interface has a well-known analogue, i.e., the dielectric/dielectric interface across which polar discontinuity exists, such as LaAlO₃/SrTiO₃ interface³⁸. The difference is that the interfacial property in the

ferroelectric/dielectric system is electrically switchable via ferroelectric switching. This enhances functional flexibility, and of course, potentially introduces more intricacies. Recently, ferroelectric switching in fe-HfO_2 has been unambiguously shown to be intertwined with electrochemically driven oxygen migration³⁹. This may either enhance or alleviate polar discontinuity, dependent on whether asymmetric oxygen distribution-induced net dipole across fe-HfO_2 has the same direction as fe-HfO_2 polarization.

In this work, we investigate several representative fe-HfO_2 /oxide dielectric interfaces by first-principles calculations. The oxide dielectrics under consideration cover a range of cation valence, electronegativity and band gaps. As a relevant interfacial effect in real device, asymmetric oxygen distribution-induced polarity, intertwined with ferroelectric polarization or not, is also investigated. With their electronic structures calculated, we discuss on their potential implications for fe-HfO_2 -based devices.

We create supercell models of several fe-HfO_2 /oxide interfaces, including $\text{fe-HfO}_2/\text{Al}_2\text{O}_3$, $\text{fe-HfO}_2/\text{La}_2\text{O}_3$, $\text{fe-HfO}_2/\text{SiO}_2$ (quartz), $\text{fe-HfO}_2/\text{GeO}_2$, $\text{fe-HfO}_2/\text{m-HfO}_2$ (m for monoclinic), $\text{fe-HfO}_2/\text{t-HfO}_2$ (t for tetragonal), $\text{fe-HfO}_2/\text{TiO}_2$, $\text{fe-HfO}_2/\text{P}_2\text{O}_5$, $\text{fe-HfO}_2/\text{Ta}_2\text{O}_5$ and $\text{fe-HfO}_2/\text{WO}_3$, each containing roughly 25 Å thick fe-HfO_2 and oxide with comparable thickness. Note that this modelled thickness value should not be viewed as being too small because fe-HfO_2 has already been scaled down to the sub-3-nm region^{34,40} and FTJ device based on 1-nm fe-HfO_2 /1-nm SiO_2 has also been demonstrated³². The fe-HfO_2 model is selected to be in the polar orthorhombic $\text{Pca}2_1$ phase which has generally been considered as the source of ferroelectricity^{41, 42}, while other ferroelectric phases have also been proposed^{43, 44}. In this fe-HfO_2 model, the displacements of the three-fold coordinated oxygen ions (O_{III^2}) along the c axis give rise to ferroelectric polarization. The electron-counting-rule is satisfied in each model. The crystalline phases of the non-ferroelectric oxides used for building the corresponding interface models are listed in supplementary table S1. The oxide slabs are cleaved along the surface orientations (listed in supplementary table S1) that provide interfacial bonding environments as compatible as possible and achieve reasonable tradeoff between lattice matching and computational burden. The in-plane lattice constants are fixed to that calculated for fe-HfO_2 single crystal, and the lattice perpendicular to the interface is relaxed, using the CASTEP code⁴⁵. The calculations use the Perdew-Burke-Ernzerhof (PBE) flavor of the generalized gradient approximation (GGA)⁴⁶, $\text{N}\times\text{M}\times 1$ Monkhorst-Pack k-points with in-plane spacing smaller than 0.067 1/Å, and ultrasoft pseudopotentials with a plane wave cutoff energy of 380 eV. Convergence test validates the parameterization, as shown in the supplementary figure S1.

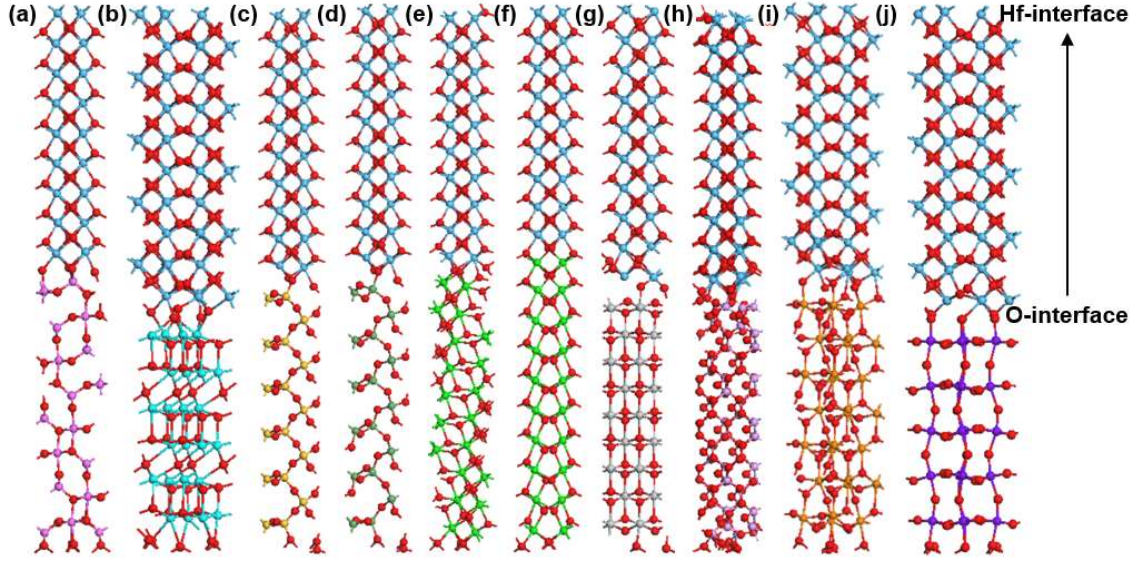


Figure 1 Atomic structures of the (a) $\text{fe-HfO}_2/\text{Al}_2\text{O}_3$, (b) $\text{fe-HfO}_2/\text{La}_2\text{O}_3$, (c) $\text{fe-HfO}_2/\text{SiO}_2$, (d) $\text{fe-HfO}_2/\text{GeO}_2$, (e) $\text{fe-HfO}_2/\text{m-HfO}_2$, (f) $\text{fe-HfO}_2/\text{t-HfO}_2$, (g) $\text{fe-HfO}_2/\text{TiO}_2$, (h) $\text{fe-HfO}_2/\text{P}_2\text{O}_5$, (i) $\text{fe-HfO}_2/\text{Ta}_2\text{O}_5$ and (j) $\text{fe-HfO}_2/\text{WO}_3$ interface systems. The arrow shows the direction of ferroelectric polarization.

In all interface models, the polarizations of fe-HfO_2 are sustained after geometry optimizations, as seen in figure 1(a-j). Each supercell model contains two interfaces that look symmetric in terms of atomic packing but actually asymmetric because of being polar. All these models are shown with the polarizations of fe-HfO_2 in the upward directions. The two asymmetric interfaces in each model with Hf^{4+} bound charge and $\text{O}_{\text{III}}^{2-}$ bound charge are referred to as the Hf-interface and O-interface, respectively. For the sake of convenience, the interface is also referred to as the end interface or the middle interface according to its position in the supercell. In models shown in figure 1, the O-interfaces are the middle interfaces and the Hf-interfaces are the end interfaces. The projected density of states (PDOS) of each model is shown in figure 2(a-j). For $\text{fe-HfO}_2/\text{m-HfO}_2$, the bands of fe-HfO_2 bend toward higher energy as they approach the O-interface. Similarly, the bands of m-HfO_2 also bend toward higher energy as they approach the O-interface. These result in wedge-shaped potential wells for electrons and holes at the Hf-interface and O-interface, respectively. The Fermi energy (E_f) of this interface system lies close to the conduction band minimums (CBMs) of fe-HfO_2 and m-HfO_2 at the Hf-interface, and lies close to their valence band maximums (VBMs) at the O-interface, indicating the tendency to form 2DEG and 2DHG, respectively. Experimentally, 2DEG and 2DHG have indeed been observed at the perovskite ferroelectric/dielectric interface system^{35, 37}.

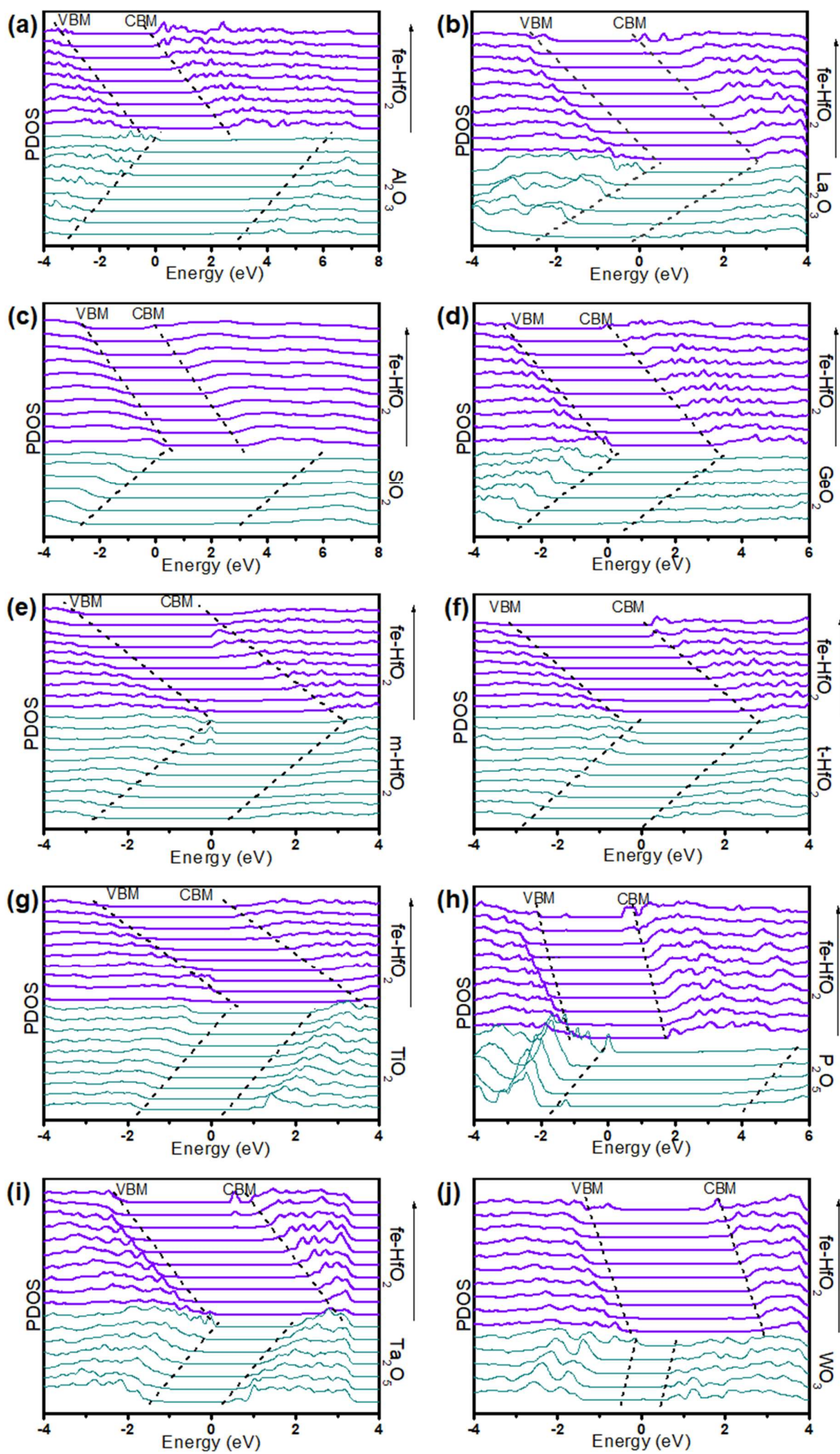


Figure 2 PDOSs of the (a) fe-HfO₂/Al₂O₃, (b) fe-HfO₂/La₂O₃, (c) fe-HfO₂/SiO₂, (d) fe-HfO₂/GeO₂, (e) fe-HfO₂/m-HfO₂, (f) fe-HfO₂/t-HfO₂, (g) fe-HfO₂/TiO₂, (h) fe-HfO₂/P₂O₅, (i) fe-HfO₂/Ta₂O₅ and (j) fe-HfO₂/WO₃ interface systems, respectively. The Fermi energies are set to 0 eV.

The direction of band bending in fe-HfO₂ indicates the existence of depolarizing field that tends to destabilize its ferroelectric polarization. In the case of fe-HfO₂/m-HfO₂, 2.2-V voltage drop across 2.7-nm fe-HfO₂ will translate to 8.3-MV/cm depolarizing field which is larger than the coercive field measured experimentally⁴⁷. Interface formation induces depolarizing field due to incomplete screening of the bound charge^{48,49}. The tendency to form 2DEG (2DHG) at the Hf-interface (O-interface) in ferroelectric/dielectric stack can be understood as a way to screen the bound charge.

Electric field in opposite direction to the depolarizing field in fe-HfO₂ is also built up in m-HfO₂. This field is also sizable, reaching 7.8 MV/cm. In some cases (see supplementary table S2 for field intensities in various fe-HfO₂/oxide interfaces), the fields in dielectrics are so strong that they could induce dielectric breakdown. It has been proposed that in practice the field in dielectric will maintain below the breakdown value because free carrier leakage through the dielectric and the ensuing trapping at the ferroelectric/dielectric interface can provide additional screening of the bound charge³¹.

Upon fe-HfO₂ ferroelectric switching, both the depolarizing field in fe-HfO₂ and the field in m-HfO₂ will change directions. It is the reversal of field and the ensuing large potential difference experienced by the m-HfO₂ layer that give rise to large TER in ferroelectric/dielectric-based FTJ device³³.

The fe-HfO₂/t-HfO₂ interface system shows similar band structure properties to those of the fe-HfO₂/m-HfO₂ system. The dynamic structural transition from m-HfO₂ or t-HfO₂ to fe-HfO₂ has been considered to be vital in giving rise to the field-cycling behavior of fe-HfO₂-based ferroelectric capacitors¹⁹. In particular, it increases the ferroelectric switching response during the wake-up phase of the device. This is easy to understand because m-HfO₂ and t-HfO₂ are not ferroelectrically active. From an interface perspective, our results also indicate that the pre-existing fe-HfO₂/m-HfO₂ and fe-HfO₂/t-HfO₂ grain boundaries will degrade the ferroelectricity in fe-HfO₂, but with gradual structural transition to fe-HfO₂ upon cycling this effect will be mitigated due to the decrease of depolarizing field.

For interfaces between fe-HfO₂ and other metal-oxide dielectrics, namely, Al₂O₃, La₂O₃, SiO₂, GeO₂, TiO₂, Ta₂O₅ and WO₃, similar interfacial band structure properties to those of fe-HfO₂/m-HfO₂ and fe-HfO₂/t-HfO₂ interfaces are found.

In periodic supercell modelling approach, a two-terminal device structure with short-circuited electrodes can be naturally modeled¹⁸. Our periodic supercell model is analogous to such a fe-

HfO₂/oxide-based device whose electrodes are ideal (zero Thomas–Fermi screening length) and infinitely thin (electrodes vanished so that fe-HfO₂ and oxide are brought together to form the end interface, due to periodicity). As introduced, each of the above supercell models is built to have the two interfaces with similar atomic packing. In doing so, the two interfaces are assumed to have equal atomic chemical potentials. However, this might not always be the case. In fact, a relatively high and low oxygen chemical potentials (μ_{O}) could exist at the fe-HfO₂/oxide interface (middle interface), and at the fe-HfO₂/electrode and oxide/electrode interfaces, respectively, in an as-fabricated device.

We simulate this condition in fe-HfO₂/SiO₂ system (the arguments developed here are very general and could be readily extrapolated to other fe-HfO₂/oxide systems) by making the middle interface O-rich and the end interface O-poor while keeping the electron-counting-rule satisfied. The difference in the number of O ions between these two interfaces is two. Bulk quartz SiO₂ is a three-dimensionally connected network with alternating short and long Si-O bonds⁵⁰. Its basic structural motif is the irregular SiO₄ tetrahedron with shared corners. GeO₂ is a network glass with similar properties to SiO₂. Compared to GeO₂, SiO₂ has less irregular SiO₄ tetrahedrons⁵¹, as seen from figure 1(c, d). In the case of fe-HfO₂ polarization pointing away from SiO₂ (up-polarization), as shown in figure 3a, depolarizing field is built up in fe-HfO₂ (figure 3b), reaching 11.8 MV/cm, which is stronger than 10.8 MV/cm in the case of equal interfacial μ_{O} . Such large depolarizing field indicates that fe-HfO₂ up-polarization is highly unfavorable. However, in the case of fe-HfO₂ down-polarization, as shown in figure 3c, hyperpolarizing (anti-depolarizing) field is built up in fe-HfO₂ (figure 3d), tending to enhance fe-HfO₂ down-polarization. Therefore, under this fabrication-relevant μ_{O} condition, the fe-HfO₂/SiO₂ system is mono-stable in zero applied field that only one of the two polarization states is stable. This mono-stability originates from the asymmetric μ_{O} at the two interfaces (forming a net dipole) and the consequential built-in field in fe-HfO₂, reminiscent of the cases in other non-ferroelectric systems^{38, 52-54}. The built-in fields in our models are strong because the μ_{O} difference between the two interfaces is large, one O per surface Hf atom. In practice, μ_{O} difference may not be that large, and may not survive annealing considering that HfO₂ is a fast oxygen ion conductor at high temperature. Experimentally, annealing is conveniently used to crystallize fe-HfO₂, and, according to our simulations, to level out μ_{O} difference and decrease the built-in field. Nevertheless, for cases in which high-temperature processes are undesired, such as flexible electronics on organic substrates, the influence of this μ_{O} difference can be significant.

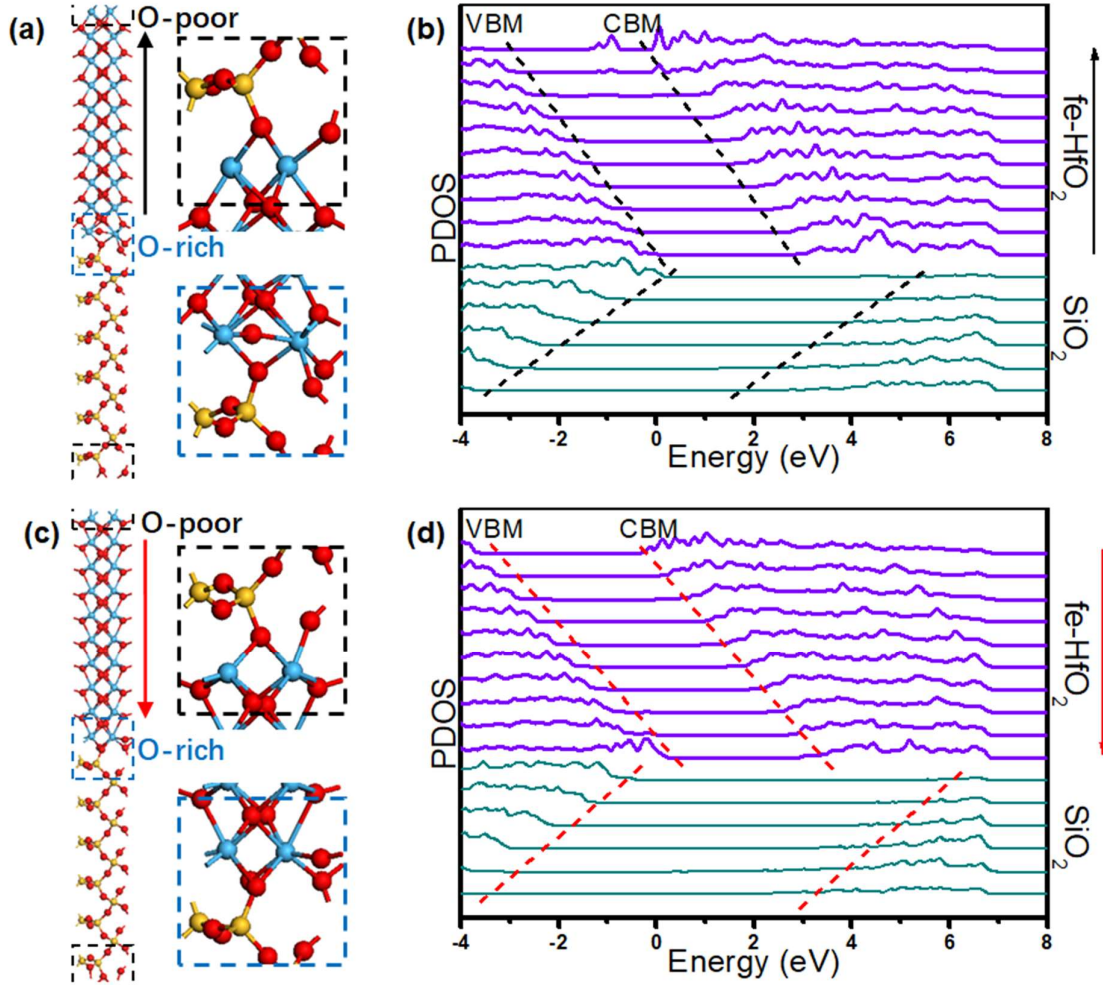


Figure 3 Atomic structure of the fe-HfO₂/SiO₂ system with O-rich middle interface and O-poor end interfaces, the fe-HfO₂ polarization is (a) upward and (c) downward. PDOSs corresponding to (b) up-polarization and (d) down-polarization configurations.

This μ_0 difference can even change dynamically with the ferroelectric switching process. It has been known that ferroelectric switching is intertwined with oxygen vacancy migration⁵⁵ and this migration can be very directional subject to electrochemical forces^{39, 56}. In the presence of such intertwined and directional oxygen vacancy migration, the O-interface will always be O-rich and the Hf-interface will always be O-poor. This is a similar case to that shown in figure 3a. The difference is that the asymmetric μ_0 distribution-induced net dipole across fe-HfO₂ changes reversibly with ferroelectric switching. Thus, both fe-HfO₂ polarization states are destabilized. This seems to impose a fundamental challenge for fe-HfO₂ devices. However, there is a compensating effect. As mentioned earlier, in the ideal fe-HfO₂/oxide system the O-interface and Hf-interface are relatively p-type and n-type, respectively, due to polarity-induced band bending (figure 1). It is known that the formation energies and charge states of point

defects are strongly dependent on the electronic chemical potential (Fermi energy). Alam et al. have shown that in fe-HfO₂ positively charged oxygen vacancies and negatively charged oxygen interstitials are thermodynamically easy to form under p-type and n-type conditions, respectively⁵⁷. These are exactly the conditions provided by the O-interface and Hf-interface in the ideal fe-HfO₂/oxide system, respectively. Therefore, the thermodynamically triggered formation of the corresponding defects at these two interfaces will partly balance out the electrochemical migration-induced difference in μ_0 . Note that polarity-induced formation of oxygen vacancy defects has been considered as a plausible mechanism in regulating the interfacial electronic structure in other non-ferroelectric systems^{58, 59}.

To conclude, we investigate several representative fe-HfO₂/oxide interfaces and find in all systems the existence of strong depolarizing field in fe-HfO₂ due to incomplete screening of the bound charge. The depolarizing field is detrimental that it destabilizes ferroelectric state, especially in the ultrathin region. Attention should be paid to this problem in developing NC-transistors and fe-transistors that uses fe-HfO₂/oxide bilayer structures. In an as-fabricated fe-HfO₂ device, the depolarizing field in fe-HfO₂ grain due to the formation of fe-HfO₂/m-HfO₂ and fe-HfO₂/t-HfO₂ grain boundaries is also an important factor influencing the device cycling behavior. Along with the depolarizing field, strong field in opposite direction is built up in oxide layer. For FTJ, the switchable electric potential across the oxide layer upon ferroelectric switching can be exploited as a source for TER³³, as long as ferroelectric polarization is not completely depolarized. As a relevant interfacial effect in real device, asymmetric oxygen distribution-induced polarity, intertwined with ferroelectric polarization or not, is also investigated. In an as-fabricated device, graded oxygen chemical potential due to different fabrication conditions results in built-in field that will make the system only mono-stable under zero applied field. This effect can be conveniently mitigated by annealing considering that HfO₂ is a good oxygen ion conductor. Related to its oxygen ion conducting property, ferroelectric switching in fe-HfO₂ is intertwined with reversible oxygen migration³⁹ that can dynamically change oxygen distribution. Despite its hidden benefits for novel electronic device functions, oxygen migration-induced net dipole across fe-HfO₂ can be troublesome in the sense of exacerbating the depolarization of fe-HfO₂. A polarity-induced interfacial defect formation mechanism is available to balance out these adversarial effects. This work provides insights into ferroelectric-HfO₂/dielectric interfaces and some useful implications for the development of devices.

Conflict of Interest

The authors declare no competing financial interest.

Acknowledgments

The authors acknowledge funding from National Natural Science Foundation (grant no. 61974082, 61704096 and 61836004). The authors acknowledge funding from National Key R&D Program of China (2018YFE0200200), Youth Elite Scientist Sponsorship (YESS) Program of China Association for Science and Technology (CAST) (no. 2019QNRC001), supercomputing wales project number sew1070, Tsinghua-IDG/McGovern Brain-X program, Beijing science and technology program (grant no. Z181100001518006 and Z191100007519009), the Suzhou-Tsinghua innovation leading program 2016SZ0102, and CETC Haikang Group-Brain Inspired Computing Joint Research Center.

DATA AVAILABILITY

The data that support the findings of this study are available from the corresponding author upon reasonable request.

References

1. Mistry K, Allen C, Auth C, et al. A 45nm Logic Technology with High-k+Metal Gate Transistors, Strained Silicon, 9 Cu Interconnect Layers, 193nm Dry Patterning, and 100% Pb-free Packaging. In: *2007 IEEE International Electron Devices Meeting*. 247-250, (2007).
2. Moore GE. Cramming more components onto integrated circuits. *IEEE Solid-State Circuits Society Newsletter*. 11, 33-35 (2006).
3. Ye P, Ernst T, Khare MV. The last silicon transistor: Nanosheet devices could be the final evolutionary step for Moore's Law. *IEEE Spectr*. 56, 30-35 (2019).
4. Sayeef S, Ni K, Suman D. The era of hyper-scaling in electronics. *Nat Electron*. 1, 442-450 (2018).
5. Böске TS, Müller J, Bräuhaus D, Schröder U, Böttger U. Ferroelectricity in hafnium oxide: CMOS compatible ferroelectric field effect transistors. In: *2011 International Electron Devices Meeting*. 24.5.1-24.5.4, (2011).
6. Böске TS, Teichert S, Bräuhaus D, et al. Phase transitions in ferroelectric silicon doped hafnium oxide. *Appl Phys Lett*. 99, 112904 (2011).
7. Salahuddin S, Datta S. Use of negative capacitance to provide voltage amplification for low power nanoscale devices. *Nano Lett*. 8, 405 (2008).
8. Alam MA, Si M, Ye PD. A critical review of recent progress on negative capacitance field-effect transistors. *Appl Phys Lett*. 114, 090401 (2019).
9. Hoffmann M, Slesazek S, Schroeder U, Mikolajick T. What's next for negative capacitance electronics? *Nat Electron*. 3, 1-3 (2020).
10. Íñiguez J, Zubko P, Luk'yanchuk I, Cano A. Ferroelectric negative capacitance. *Nat Rev Mater*. 4, 243-256 (2019).
11. Khan AI, Keshavarzi A, Datta S. The future of ferroelectric field-effect transistor technology. *Nat Electron*. 3, 588-597 (2020).

12. Mikolajick T, Slesazek S, Mulaosmanovic H, Park MH, Schroeder U. Next generation ferroelectric materials for semiconductor process integration and their applications. *J Appl Phys.* 129, 100901 (2021).
13. Chen A. A review of emerging non-volatile memory (NVM) technologies and applications. *Solid-State Electron.* 125, 25-38 (2016).
14. Daniele I, Philip HS. In-memory computing with resistive switching devices. *Nat Electron.* 1, 333-343 (2018).
15. Tsymbal E, Kohlstedt H. Tunneling Across a Ferroelectric. *Science (New York, NY).* 313, 181-3 (2006).
16. Garcia V, Bibes M. Ferroelectric tunnel junctions for information storage and processing. *Nat Commun.* 5, 4289 (2014).
17. Dawber M, Rabe KM, Scott JF. Physics of thin-film ferroelectric oxides. *Rev Mod Phys.* 77, 1083-1130 (2005).
18. Junquera J, Ghosez P. Critical thickness for ferroelectricity in perovskite ultrathin films. *Nature.* 422, 506-509 (2003).
19. Pešić M, Fengler FPG, Larcher L, et al. Physical Mechanisms behind the Field-Cycling Behavior of HfO₂-Based Ferroelectric Capacitors. *Adv Funct Mater.* 26, 4601-4612 (2016).
20. Ma Z, Zhang Q, Valanoor N. A perspective on electrode engineering in ultrathin ferroelectric heterostructures for enhanced tunneling electroresistance. *Applied Physics Reviews.* 7, 041316 (2020).
21. Cheng CH, Chin A. Low-Voltage Steep Turn-On pMOSFET Using Ferroelectric High- κ Gate Dielectric. *IEEE Electron Device Lett.* 35, 274-276 (2014).
22. Lee MH, Chen PG, Liu C, et al. Prospects for ferroelectric HfZrOx FETs with experimentally CET=0.98nm, SS_{for}=42mV/dec, SS_{rev}=28mV/dec, switch-off <0.2V, and hysteresis-free strategies. In: *2015 IEEE International Electron Devices Meeting (IEDM).* 22.5.1-22.5.4, (2015).
23. Li KS, Chen PG, Lai TY, et al. Sub-60mV-swing negative-capacitance FinFET without hysteresis. In: *2015 IEEE International Electron Devices Meeting (IEDM).* 22.6.1-22.6.4, (2015).
24. Nourbakhsh A, Zubair A, Joglekar S, Dresselhaus M, Palacios T. Subthreshold swing improvement in MoS₂ transistors by the negative-capacitance effect in a ferroelectric Al-doped-HfO₂/HfO₂ gate dielectric stack. *Nanoscale.* 9, 6122-6127 (2017).
25. Si M, Su C-J, Jiang C, et al. Steep-slope hysteresis-free negative capacitance MoS₂ transistors. *Nat Nanotechnol.* 13, 24-28 (2018).
26. Ni K, Yin X, Laguna AF, Joshi S, Datta S. Ferroelectric ternary content-addressable memory for one-shot learning. *Nat Electron.* 2, 521-529 (2019).
27. Myungsoo S, Kang MH, Seung-Bae J, et al. First Demonstration of a Logic-Process Compatible Junctionless Ferroelectric FinFET Synapse for Neuromorphic Applications. *IEEE Electron Device Lett.* 39, 1445-1448 (2018).
28. Jerry M, Chen P, Zhang J, et al. Ferroelectric FET analog synapse for acceleration of deep neural network training. In: *2017 IEEE International Electron Devices Meeting (IEDM).* 6.2.1-6.2.4, (2017).
29. Dutta S, Schafer C, Gomez J, Ni K, Datta S. Supervised Learning in All FeFET-Based Spiking Neural Network: Opportunities and Challenges. *Front Neurosci.* 14, 634 (2020).

30. Berdan R, Marukame T, Ota K, et al. Low-power linear computation using nonlinear ferroelectric tunnel junction memristors. *Nat Electron.* 3, 1-8 (2020).
31. Si M, Xiao L, Ye PD. Ferroelectric Polarization Switching of Hafnium Zirconium Oxide in a Ferroelectric/Dielectric Stack. *ACS Appl Electron Mater.* 1, 745-751 (2019).
32. Cheema SS, Shanker N, Hsu C-H, et al. One Nanometer HfO₂-Based Ferroelectric Tunnel Junctions on Silicon. *Adv Electron Mater.* n/a, 2100499 (2021).
33. Zhuravlev M, Wang Y, Maekawa S, Tsymbal E. Tunneling Electroresistance in Ferroelectric Tunnel Junctions with a Composite Barrier. *Appl Phys Lett.* 95, (2009).
34. Cheema SS, Kwon D, Shanker N, Reis RD, Salahuddin S. Enhanced ferroelectricity in ultrathin films grown directly on silicon. *Nature.* 580, 478-482 (2020).
35. Zhang Y, Lu H, Xie L, et al. Anisotropic polarization-induced conductance at a ferroelectric-insulator interface. *Nat Nanotechnol.* 13, 1132-1136 (2018).
36. Niranjana MK, Wang Y, Jaswal SS, Tsymbal EY. Prediction of a Switchable Two-Dimensional Electron Gas at Ferroelectric Oxide Interfaces. *Phys Rev Lett.* 103, 016804 (2009).
37. Huyan H, Addiego C, Yan X, et al. Direct observation of polarization-induced two-dimensional electron/hole gases at ferroelectric-insulator interface. *npj Quantum Mater.* 6, 88 (2021).
38. Nakagawa N, Hwang HY, Muller DA. Why some interfaces cannot be sharp. *Nat Mater.* 5, 204-209 (2006).
39. Nukala P, Ahmadi M, Wei Y, et al. Reversible oxygen migration and phase transitions in hafnia-based ferroelectric devices. *Science.* 372, 630-635 (2021).
40. Tian X, Shibayama S, Nishimura T, Yajima T, Migita S, Toriumi A. Evolution of ferroelectric HfO₂ in ultrathin region down to 3 nm. *Appl Phys Lett.* 112, 102902 (2018).
41. Sang X, Grimley ED, Schenk T, Schroeder U, Lebeau JM. On the structural origins of ferroelectricity in HfO₂ thin films. *Appl Phys Lett.* 106, 114113 (2015).
42. Xu X, Huang F-T, Qi Y, et al. Kinetically stabilized ferroelectricity in bulk single-crystalline HfO₂:Y. *Nat Mater.* 20, 826-832 (2021).
43. Huan TD, Sharma V, Rossetti GA, Ramprasad R. Pathways Towards Ferroelectricity in Hafnia. *Phys Rev B.* 90, 064111 (2014).
44. Wei Y, Nukala P, Salverda M, et al. A rhombohedral ferroelectric phase in epitaxially strained Hf_{0.5}Zr_{0.5}O₂ thin films. *Nat Mater.* 17, 1095-1100 (2018).
45. Clark SJ, Segall MD, Pickard CJ, et al. First principles methods using CASTEP. *Z Kristallogr Cryst Mater.* 220, 567-570 (2005).
46. Perdew JP, Burke K, Ernzerhof M. Generalized Gradient Approximation Made Simple. *Phys Rev Lett.* 77, 3865-3868 (1996).
47. Materano M, Lomenzo P, Mulaosmanovic H, et al. Polarization switching in thin doped HfO₂ ferroelectric layers. *Appl Phys Lett.* 117, 262904 (2020).
48. Tagantsev AK, Gerra G. Interface-induced phenomena in polarization response of ferroelectric thin films. *J Appl Phys.* 100, 2623-314 (2006).
49. Bernardini F, Fiorentini V. Polarization fields in nitride nanostructures: ten points to think about. *Appl Surf Sci.* 166, 23-29 (2000).
50. Feigl FJ, Fowler WB, Yip KL. Oxygen vacancy model for the E₁' center in SiO₂. *Solid State Commun.* 14, 225-229 (1974).

51. G. S. Smith and P. B. Isaacs, The crystal structure of quartz-like GeO₂, *Acta Cryst.* 17, 842-846 (1964)
52. Lee H, Campbell N, Lee J, et al. Direct observation of a two-dimensional hole gas at oxide interfaces. *Nat Mater.* 17, 231-236 (2018).
53. Lin L, Li H, Robertson J. Control of Schottky barrier heights by inserting thin dielectric layers. *Appl Phys Lett.* 101, 172907 (2012).
54. Cheng D, Kong D, Sheng X, Yin L, Li H. Perovskite hetero-anionic-sublattice interfaces for optoelectronics and nonconventional electronics. *Nanoscale.* 12, 7263 (2020).
55. Starschich S, Menzel S, Böttger U. Evidence for oxygen vacancies movement during wake-up in ferroelectric hafnium oxide. *Appl Phys Lett.* 108, 032903 (2016).
56. Lü W, Li C, Zheng L, et al. Multi-Nonvolatile State Resistive Switching Arising from Ferroelectricity and Oxygen Vacancy Migration. *Adv Mater.* 29, 1606165 (2017).
57. Alam MNK, Clima S, O'Sullivan BJ, et al. First principles investigation of charge transition levels in monoclinic, orthorhombic, tetragonal, and cubic crystallographic phases of HfO₂. *J Appl Phys.* 129, 084102 (2021).
58. Zhang L, Zhou X-F, Wang H-T, et al. Origin of insulating behavior of the p-type LaAlO₃/SrTiO₃ interface: Polarization-induced asymmetric distribution of oxygen vacancies. *Phys Rev B.* 82, (2010).
59. Yu L, Zunger A. A polarity-induced defect mechanism for conductivity and magnetism at polar–nonpolar oxide interfaces. *Nat Commun.* 5, 5118 (2014).